The intergalactic medium near high-redshift galaxies

Rakic, O.

5

How much H I Lyα Absorption near Galaxies at $z \approx 2.4$ is due to Cold Flows?

Inspired by recent studies that suggest that galaxies grow primarily by acquiring gas through cold accretion, we studied the covering fraction of Lyα absorbing gas with different properties within 200 proper kpc from haloes with masses $M_{\rm h} \geq 10^{11.5}$ M$_\odot$, which are thought to host Lyman Break type galaxies at redshift $z \approx 2.4$. We use a cosmological hydrodynamical simulation with radiative transfer applied in post-processing. We consider the contributions to the absorption of different gas samples, selected on the basis of the maximum past temperature, halo membership, and past, current and future relation to the interstellar medium. We also examine the median optical depth that the different gas samples produce on 3-D distance scales $\lesssim 5$ proper Mpc. We find that gas with a maximum past temperature of $T_{\rm max} < 10^{5.5}$ K accounts for almost all the absorption. The contribution of gas residing in the halo increases with declining distance to galaxies and with the strength of the absorber. The majority of gas, on all scales, is moving towards the haloes. While outflowing and static gas have similar and non-negligible covering fractions close to haloes, the contribution of outflowing gas declines with distance, while absorption by static gas exceeds that of inflowing gas at ~ 5 pMpc from galaxies. Most of the Lyα absorbing gas within 200 pkpc will enter the ISM of galaxies by $z = 0$, and most of it will do so for the first time. Gas that is at $\gtrsim 500$ proper kpc from haloes will not enter the ISM by $z = 0$. Gas with $T_{\rm max} < 10^{5.5}$ K, as well as infalling gas, and gas that will join galaxies by $z = 0$ can account for the observed covering fraction of Lyα absorbing gas. Gas with $T_{\rm max} < 10^{5.5}$ K in addition has a median optical depth consistent with that observed at distances $\gtrsim 200$ pkpc. We also examine the temperature and density of Lyα absorbing gas as a function of distance from the galaxy in simulations with and

without SN and AGN feedback, and find that galactic feedback is the main culprit in heating gas to $T \gtrsim 10^5$ K close to galaxies, although gravitational shock-heating is a non-negligible effect. Strong feedback can affect the state of the IGM out to ~ 2 proper Mpc from galaxies through heating of gas by winds emanating from galaxies in the same general region, causing an inversion of the temperature-density relation, which provides another way to constrain galactic feedback effects through measurements of the spatially resolved IGM temperature.

5.1 Introduction

Recent theoretical efforts imply that most of the fuel for star-formation comes into galaxies through "cold accretion flows", which consist of gas that did not shock-heat to the virial temperature when it accreted onto the host halo (e.g. Birnboim & Dekel 2003; Kereš et al. 2005, 2009; Ocvirk et al. 2008; Brooks et al. 2009; Crain et al. 2010; Van de Voort et al. 2011a,b; Faucher-Giguere et al. 2011). Instead, this gas falls in while maintaining a temperature of $\sim 10^4$ K, although it may shock heat to much higher temperatures if and when it accretes onto the galaxy. Simulations show that this "cold mode" gas typically falls in through filaments which can penetrate haloes of hot, hydrostatic or outflowing gas. In this chapter we examine how much of the H I Lyα absorption close to galaxies is due to this material.

Recent results of Van de Voort et al. (2011a) are based on the simulations from the same suite of OverWhelmingly Large Simulations (OWLS; Schaye et al. 2010) as the work presented in this chapter, so here we provide a short summary of their findings. They found that gas accretion is bimodal, with maximum past temperatures being either of order the virial temperature, or $\lesssim 10^5$ K. This is a consequence of the cooling function having a maximum at $T \approx 10^{5-5.5}$ K (e.g. Wiersma et al. 2009a). Van de Voort et al. (2011a) also find that the rate of accretion onto galaxies is smaller than the accretion rate onto haloes, and that this difference increases with time. It is worth noting that the ratio between the accretion rates onto haloes and galaxies is minimal for $M_{\rm halo} \sim 10^{12}\,{\rm M}_\odot$ (and at $z = 2$ this ratio equals 2), which falls in the range of typical masses of dark matter halo hosts of the LBG-type galaxies at $z \approx 2-3$ (Chapter 4). The importance of gas accreted in the hot mode increases with halo mass and towards lower redshifts. When it comes to accretion onto halos, cold accretion dominates for halos with $M_{\rm h} \ll 10^{12}\,{\rm M}_\odot$, and hot accretion for $M_{\rm h} \gg 10^{12}\,{\rm M}_\odot$, and the relative importance of the two is robust to changes in feedback and cooling prescriptions. On the other hand, when it comes to accretion onto galaxies, the cold mode is always important, and for all halo masses and at all redshifts most of the stars were on average formed from gas accreted in the cold mode. Stars formed from hot-mode gas account for only $\sim 20\%$ of the stellar mass of galaxies in halos with $M_{\rm h} \gtrsim 10^{11.5}{\rm M}_\odot$ at $z \approx 2$. For accretion onto galaxies, the relative importance of the two modes is more sensitive to feedback and cooling prescriptions than for accretion onto halos.

Several publications have recently made predictions for the absorption signatures of cold flows. They in general either give predictions useful for observations of QSO-galaxy pairs, or for "down the barrel" absorption signatures, i.e. for absorption in spectra of the galaxies onto which gas is being accreted. Faucher-Giguere & Kereš (2011) use Smoothed Particle Hydrodynamics (SPH) simulations to find the covering fraction of Lyman Limit Systems (LLSs; $N_{\rm HI} \geq 10^{17.2}\,{\rm cm}^{-2}$) and Damped Lyman Alpha systems

(DLAs; $N_{\rm HI} \geq 10^{20.3}\,{\rm cm}^{-2}$) within 0.5, 1, and 2 $R_{\rm vir}$ of a galaxy halo ($M_{\rm h} = 3.2 \times 10^{11}\,{\rm M}_{\odot}$ at $z = 2$) at redshifts $z = 2$, 3, and 4. Their simulations do not include any galactic feedback. They do not track the gas history and can therefore not distinguish between currently cool gas accreted through the hot and cold modes. Kimm et al. (2011) and Fumagalli et al. (2011) used AMR simulations to examine, among other things, the covering fraction of cold gas for haloes of different masses and at different redshifts. They also do not take gas history into account (which would also be impossible due to the Eulerean nature of their simulations). Stewart et al. (2011a,b) used cosmological SPH simulations to study the covering fraction of cold gas (also without looking at the gas history) within 50 comoving kpc of galaxies residing in Milky Way type progenitor haloes ($M_{\rm h}(z = 0) = 1.4 \times 10^{12}$), from redshift $z \approx 4$ to 0. While their predictions are useful for galaxy-galaxy pair observations, it will be extremely challenging to build a statistical sample of QSO-galaxy pairs with such small separations at high z. Indeed, the smallest separation in the sample used by Rakic et al. (2011) and Rudie et al. (in preparation) is ≈ 55 kpc physical. Using QSOs, as opposed to galaxies, as background sources is, however, important if one wants to study lower columns of gas than is possible with spectra of background galaxies which are generally of much lower quality than those of QSOs.

Van de Voort et al. (2011c) used the reference simulation from the OWLS suite, post-processed with radiative transfer, to study the nature of high column density ($N_{\rm HI} \geq 10^{16}\,{\rm cm}^{-2}$) Ly$\alpha$ absorbers at $z = 3$. They computed the contributions to the H I columns of gas selected in terms of its maximum past temperature, whether it is in haloes, its kinematics with respect to the haloes, and participation in star formation in the past, present and future. They found that gas with a maximum past temperature of $T_{\rm max} \leq 10^{5.5}$ K accounts for almost all absorption in systems with $N_{\rm HI} \geq 10^{16}\,{\rm cm}^{-2}$, and that gas accreted in the "hot mode" is only important for very strong absorbers, $N_{\rm HI} \geq 10^{21}\,{\rm cm}^{-2}$. Considering this, they concluded that the cold flows have already been detected in the form of high column density systems. The likelihood of halo membership increases with the absorption strength, and $\gtrsim 80\%$ of absorbers with $N_{\rm HI} \geq 10^{18}\,{\rm cm}^{-2}$ reside within haloes. Gas moving towards the nearest (in units of $R_{\rm vir}$) halo with a velocity, $v_{\rm gas}$, larger than 1/4 of the circular velocity, $v_{\rm circ}$, of the halo accounts for $\sim 60\%$ of the absorption, while gas outflowing with $v_{\rm gas} \geq 0.25 v_{\rm circ}$ accounts for $\sim 20\%$ of the absorption. The ISM dominates the absorption only for $N_{\rm HI} \geq 10^{21}\,{\rm cm}^{-2}$. The chance of having been part of the ISM before ("recycled gas") or after the moment of observation ($z = 3$) increases with absorption strength. About 70% of the gas in $N_{\rm HI} \geq 10^{17} - 10^{21}\,{\rm cm}^{-2}$ systems enters a galaxy by $z = 2$, $\lesssim 40\%$ has been recycled, and $\lesssim 35\%$ will enter galaxies after $z = 3$ for the first time. They also found that haloes with total mass $< 10^{10}\,{\rm M}_{\odot}$ dominate the absorption for $10^{17} < N_{\rm HI} < 10^{21}\,{\rm cm}^{-2}$.

Although the idea that cold flows dominate the fueling of galaxies is

strongly supported by cosmological hydrodynamical simulations, it has, as of yet, no conclusive backing in the observations. In fact, spectra of star-forming galaxies show only clear signs of outflows, at both high (e.g. Pettini et al. 2001; Adelberger et al. 2003, 2005; Shapiro et al. 2009; Weiner et al. 2009; Steidel et al. 2010) and low redshift (e.g. Martin & Bouche 2009; Chen et al. 2010). At the same time, there is circumstantial evidence that gas replenishment is needed to provide the necessary fuel for the measured build-up of stellar mass (e.g. Papovich et al. 2010) and to explain the relationship between stellar mass and metallicity (Erb et al. 2006; Erb 2008), and the HI gas density (non)evolution from $z \approx 2$ to $z = 0$ (Prochaska et al. 2009).

Ribaudo et al. (2011) discovered a metal-poor Lyman limit system (LLS) at $z = 0.27395$, separated by only 37 kpc from a star-forming galaxy at an almost identical redshift, and they suggest that its low metallicity ([Mg/H] $= -1.71 \pm 0.06$) makes it consistent with being cold accretion. However, association with an undetected dwarf galaxy, although unlikely, cannot be completely ruled out, and a low metallicity does not guarantee that the gas is accreting. Giavalisco et al. (2011) have also recently reported the discovery of a large amount of cold, metal-poor gas in an overdensity of galaxies at $z \approx 1.6$. They suggest, based on the analysis of the co-added absorption spectra of background galaxies, that this gas is potentially undergoing infall onto the background overdensity and its galaxies, which they say is a tentative detection of cold accretion. Dijkstra & Loeb (2009) and Goerdt et al. (2010) claimed that Lyα blobs at $z \sim 3$ (e.g. Steidel et al. 2000, 2011) may be cooling radiation from cold flows. However, simulations by Furlanetto et al. (2005) and Faucher-Giguere et al. (2010) suggest that cooling radiation is insufficient to explain Lyα blob luminosities, which is also what Steidel et al. (2011) concluded based on stacked narrow-band observations of star-forming galaxies at $z \approx 2.65$. Instead, these authors suggested that the blobs are fully consistent with being powered by the light of central objects that is scattered by surrounding gas. Finally, Hayes et al. (2011) measured a high polarization for the Lyα radiation from the blobs which supports the idea that they are powered by a central source.

Motivated by the recent observations of Rakic et al. (2011) who studied the distribution of Lyα absorbing gas around $\langle z \rangle \approx 2.36$ star-forming galaxies, we use SPH simulations to determine how much of the absorption that they measured could be due to cold accretion gas. They found the Lyα absorption to be enhanced out to at least 2.8 Mpc proper from galaxies (3σ confidence). They also found evidence of gas infall into the overdensities occupied by galaxies. The observed infall manifests itself as a compression of the absorption signal along the LOS, i.e. the absorption is enhanced out to at least 2 Mpc in the transverse direction from galaxies, but only out to ≈ 1.5 Mpc along the LOS. These scales are large in comparison with the virial radius of the galaxies ($R_{\rm vir} \approx 100$ kpc), and therefore the observed infall could not be considered "cold accretion", in the sense that separation

into cold and hot mode is possible only on scales $\lesssim R_{\rm vir}$. Nevertheless, it is the only observation that unequivocally proves that gas is moving towards galaxies. We analyze the OWLS simulations, which are particularly well suited for this type of study because their Lagrangian nature allows one to trace back the history of the gas. The maximum past temperature, $T_{\rm max}$, and the redshift when it was reached, $z_{\rm max}$, are saved for each particle. This allows us to distinguish between particles that did and those that did not go through an accretion shock near the virial radius. In comparison with most earlier works, we improve by differentiating between absorption that comes from gas with particular past properties, kinematics with respect to nearby haloes, membership of a halo, and participation in ISM of galaxies. In comparison with Van de Voort et al. (2011c), we complement their work by considering the spatial distribution of gas with respect to galaxies, while they studied global properties of absorbers, and we also study weaker absorbers ($N_{\rm HI} \ll 10^{16}\,{\rm cm}^{-2}$) along with strong ones ($N_{\rm HI} \geq 10^{16}\,{\rm cm}^{-2}$), while they focused only on stronger systems. In addition, we focus on haloes with $M_{\rm h} > 10^{11.5}\,{\rm M}_{\odot}$ whose virial temperatures are $> 10^{5.5}$ K, and are therefore suitable places to look for cold accretion streams penetrating hot haloes.

In the first part of this chapter we will consider the contribution to the absorption of gas with different kinematics, past temperature, halo membership, and participation in the ISM at any time in the history of the Universe. In the second part of the chapter we will study the physical properties of the Lyα absorbing gas, i.e. the temperature and density, as a function of the distance from the haloes. We will also examine how sensitive these properties are to changes in feedback prescriptions in the simulations.

We describe the simulations in Section 5.2. We show how much of the absorption on scales $\sim R_{\rm vir}$ is produced by gas with various properties in Section 5.3, and we do the same for absorption on larger scales ($\gg R_{\rm vir}$) in Section 5.4. In Section 5.5 we look into the temperature and density of Lyα absorbing gas in different models. We conclude in Section 5.6.

We denote proper distances as pMpc and pkpc, and comoving distances as cMpc and ckpc.

5.2 Simulations

We rely mostly on the "reference" (*REF*) simulation from the suite of OverWhelmingly Large Simulations (OWLS; Schaye et al. 2010). The simulation is run in a 50 h^{-1} cMpc box, containing 2×512^3 dark matter and baryonic particles. The simulations were already briefly described in Chapter 4. This is the only model we use in the first part of this chapter where we study absorption by cold flows. In the second part of the chapter, which investigates the physical properties of the Lyα absorbing gas, we also make use of the *AGN* model, which was also described in the previous chapter, to study the effect of very strong feedback. We will use the *NOSN* model, which

is identical to the *REF* model except that it does not contain supernova (SN) feedback, to determine how much gas heating comes from gravitational shock-heating, and how much is due to galactic winds.

In the first part of the chapter we use the *REF* model with radiative transfer of ionizing radiation applied in post-processing, while no such treatment was applied to the simulations used in the second part of the chapter.

5.2.1 Radiative transfer in post-processing

The gas in the OWLS simulations is exposed to the cosmic microwave background and to the ionizing background radiation from galaxies and quasars according to the model from Haardt & Madau (2001), but this is done in the optically thin limit where each gas particle, irrespective of its density, is subject to the same radiation intensity. This is an excellent approximation for gas with column densities $N_{\rm HI} \lesssim 10^{17}\,{\rm cm}^{-2}$, but gas at higher densities can self-shield against the ionizing radiation, in which case it reaches higher neutral fractions than in the optically thin limit. Given that we are interested in gas, accreting onto dark matter halos and their galaxies and that this gas might reach relatively high densities, we post-process the $z = 2.25$ snapshot from the simulation with radiative transfer, as described in Altay et al. (2011, and in preparation). Note that local sources of radiation were ignored.

Altay et al. (2011) used the *REF* model from the OWLS suite of simulations, which is identical to the one used here, except that their simulation was run with WMAP7 cosmological parameters, as opposed to WMAP3 in our case, and that they used a 25 h^{-1} cMpc rather than a 50 h^{-1} cMpc box. After applying the radiative transfer calculation with self-shielding, they found that the *REF* model reproduces the observed $z = 3$ properties of Lyα absorbers, i.e. the abundance of Lyα forest lines, LLSs, and DLAs, spanning over ten orders of magnitude in H I column density.

5.2.2 Thermal history of gas particles

The maximum temperature ever reached is recorded for every time step for each particle in the OWLS simulations. Given that the simulations have insufficient resolution to properly treat the interstellar medium (ISM), any gas particle with density $n_{\rm H} \geq 0.1\,{\rm cm}^{-3}$ is assumed to be part of the ISM, multi-phase and star-forming, and its pressure is imposed in the form of a polytropic equation of state $P \propto n_{\rm H}^{4/3}$. The temperature of such gas just reflects the imposed equation of state, and therefore the maximum recorded temperature does not get updated as long as the particle is part of the ISM.

Since we can follow the thermal history of the gas, we can study, for example, how much absorption at $z = 2.25$ is produced by gas that has never reached temperatures higher than some threshold value, that is inside haloes

and infalling onto galaxies at a given velocity, or is found to have been a part of the ISM before, at, or after $z = 2.25$. Table 5.1 summarizes all the selection criteria that we consider in this Chapter.

We chose the maximum past temperature of $T = 10^{5.5}$ K as the threshold temperature separating cold and hot accretion, because this is where the cooling function has its maximum (e.g. Wiersma et al. 2009a), and because Van de Voort et al. (2011a) found that this value best separates the cold and hot accretion modes. The virial temperature of haloes, $T_{\rm vir}$, is defined as follows:

$$T_{\rm vir} = \left(\frac{G^2 H_0^2 \Omega_{\rm m} 18\pi^2}{54}\right)^{1/3} \frac{\mu m_{\rm H}}{k_{\rm B}} M_{\rm halo}^{2/3} (1+z)$$
$$\approx 10^6 \,{\rm K} \left(\frac{\mu}{0.59}\right) \left(\frac{M_{\rm halo}}{10^{12} {\rm M}_\odot}\right)^{2/3} \left(\frac{1+z}{3.4}\right) \quad (5.1)$$

where G is the gravitational constant, H_0 the Hubble constant, μ the mean molecular weight, $m_{\rm H}$ the mass of a hydrogen atom, and $k_{\rm B}$ Boltzmann's constant. While the stated definition of hot and cold accretion is not appropriate for haloes with virial temperatures lower than $10^{5.5}$ K, i.e. $M_{\rm h} \lesssim 10^{11.2}$ M$_\odot$, since in this regime it becomes impossible to determine whether gas has gone through the shock or not (i.e. its maximum past temperature is similar to the virial temperature of such haloes), it is fine for our mass range of interests, $M_{\rm h} \gtrsim 10^{11.5}$ M$_\odot$, with virial temperatures of $\gtrsim 10^{5.7}$ K at $z = 2.4$.

5.2.3 Observing simulations

Similar to the procedure described in Chapter 4, we compute H I Lyα absorption spectra for 12,500 sightlines randomly drawn within 5 pMpc from haloes with masses $M_{\rm h} > 10^{11.5}$ M$_\odot$, and within 200 pkpc we draw an additional 6000 sightlines in order to sample the immediate halo surroundings sufficiently well. The distribution of impact parameters is uniform as a function of radius. This mass threshold was chosen because in the same chapter we found haloes with masses $M_{\rm h} > 10^{11.5}$ M$_\odot$ to be the most likely hosts of the galaxy population used in Rakic et al. (2011). This procedure is repeated for each gas sample listed in Table 5.1, where the density of particles not satisfying the stated conditions is set to zero. Due to the uncertainty in the intensity of the ionizing background radiation, we rescale the optical depth in the default case, i.e. when including all gas, to match the median optical depth in the observations of Rakic et al. (2011), $\log_{10}\tau_{{\rm Ly}\alpha} = -1.27$. For the rest of the variations listed in Table 5.1 we use the multiplication factor as determined for the default case. We use a subset of selections from Van de Voort et al. (2011c), where more details about the selection of particles can be found.

We use the Friends-of-Friends (FoF) algorithm to identify haloes. Two particles belong to the same group if their separation is less than 20% of the

Table 5.1 – List of applied cuts. The first column states the conditions that gas particles need to satisfy with respect to their maximum past temperature, whether they are inside halos with $M_{\rm h} > 10^{11.5}$ $M_\odot$, whether they are infalling/outflowing with respect to the nearest such halo, and whether they are part of the ISM at, after, or before $z = 2.25$. In the second column we give global fraction of the gas mass satisfying the stated conditions.

Variations	Global gas fraction
All particles - default case	1.000
$T_{\rm max} \leq 10^{5.5}$ K	0.882
In haloes ($M_{\rm h} \geq 10^{11.5}$ $M_\odot$)	0.024
In haloes ($M_{\rm h} \geq 10^{11.5}$ $M_\odot$), infall with $v > 0.25 v_{\rm circ}$	0.012
In haloes ($M_{\rm h} \geq 10^{11.5}$ $M_\odot$), outflow with $v > 0.25 v_{\rm circ}$	0.004
In haloes ($M_{\rm h} \geq 10^{11.5}$ $M_\odot$), static, i.e. $v < 0.25 v_{\rm circ}$	0.008
Infall toward the nearest (in units of $R_{\rm vir}$) halo ($M_{\rm h} \geq 10^{11.5}$ $M_\odot$), with $v > 0.25 v_{\rm circ}$	0.480
Outflow from the nearest (in units of $R_{\rm vir}$) halo ($M_{\rm h} \geq 10^{11.5}$ $M_\odot$), with $v > 0.25 v_{\rm circ}$	0.056
Static w.r.t. the nearest (in units of $R_{\rm vir}$) halo ($M_{\rm h} \geq 10^{11.5}$ $M_\odot$), i.e. $v < 0.25 v_{\rm circ}$	0.463
Gas particles that are in the ISM at $z = 2.25$	0.015
Gas particles that became ISM after $z = 2.25$	0.104
Gas particles that became ISM after $z = 2.25$ for the first time	0.069
Gas particles that were in the ISM before, but are not at $z = 2.25$	0.035

average inter-particle separation. Such groups have an average overdensity typical for virialized objects, i.e. $\langle \rho_{\rm halo} \rangle / \langle \rho \rangle \approx 180$ (e.g. Lacey & Cole 1994). A baryonic particle belongs to the same halo as its nearest dark matter particle.

The positions and masses of haloes are determined using a spherical overdensity criterion as implemented in the SubFind algorithm (Dolag et al. 2009). The position of a halo is taken to be the position of its most bound particle. The virial radius, $R_{\rm vir}$, is estimated by requiring that the enclosed density agrees with the top-hat spherical collapse approximation (Bryan & Norman 1998). The virial mass, $M_{\rm vir}$, is the total mass within $R_{\rm vir}$.

For some of the gas samples listed in Table 5.1 we consider whether particles are moving with respect to the nearest halo with $M_{\rm h} > 10^{11.5}$ $M_\odot$, in units of $R_{\rm vir}$. In other words, distances towards a halo, d, are normalized by $R_{\rm vir}$, and the nearest halo is one for which $d/R_{\rm vir}$ has minimum. The halo circular velocity is defined as $v_{\rm circ} = \sqrt{G M_{\rm vir}/R_{\rm vir}}$.

To allow comparison with observations of Rakic et al. (2011) and Rudie et al. (2011, in preparation) whose galaxies have measured redshift errors of $\pm 125\,{\rm km\,s^{-1}}$, we add random errors from a Gaussian distribution, $\sigma = 125\,{\rm km\,s^{-1}}$, to the line of sight positions of haloes in the simulations (i.e. along only one dimension that is parallel to the line of sight).

Figure 5.1 shows example spectra along a sightline that passes 69 pkpc

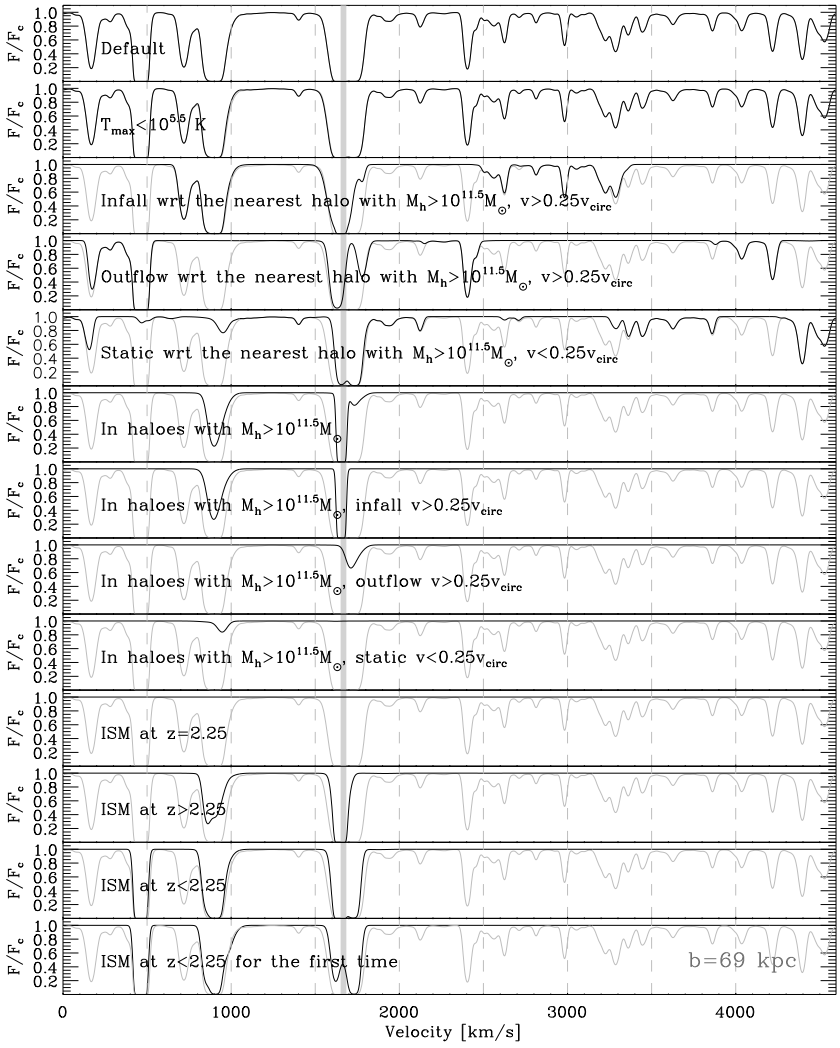

Figure 5.1 – Spectra along a LOS that passes 69 kpc from a nearby halo with total mass $M_{\rm h} = 10^{11.74}$ M$_\odot$ at $z = 2.25$, whose position is indicated by the grey vertical stripe. Different panels show the spectra for different gas samples. The fourth panel from the bottom shows no absorption, because the ISM gas is concentrated in the centers of haloes, and to have such gas at $b = 69$ pkpc it is necessary to intersect a neighboring galaxy, which is not the case for this sightline. The default case (all gas, top panel) is repeated in each panel in grey.

from a nearby halo of mass $M_{\rm h} = 10^{11.74}$ M$_\odot$, for the gas samples listed in Table 5.1. By comparing absorption in different gas samples with the

default case (i.e. where all particles are included), it can be seen that the majority of Lyα forest lines originate in gas that was never shock-heated to temperatures $T > 10^{5.5}\,\mathrm{K}$, and is not in haloes. In addition, very few lines originate in gas that becomes part of the ISM. In the next sections we will quantify the contributions from these different IGM components to the H I Lyα absorption near galaxies.

5.3 Circum-galactic medium

As already discussed in Chapter 3, when it comes to stronger absorbers, which we expect to be close to galaxies, it is more appropriate to measure their strength in terms of their central optical depth or column density, instead of the median optical depth. Using the median optical depth within a given velocity interval might underestimate the amount of neutral gas, and is very dependent on the size of the region over which the median is estimated. We look both into the covering fraction of sightlines as a function of the maximum optical depth within a given distance from galaxies, and into the covering fraction as a function of the H I column density. We use the former for absorbers that are optically thin to the ionizing radiation ($N_{\mathrm{HI}} < 10^{17.2}\,\mathrm{cm}^{-2}$, or $\log_{10}\tau_{\mathrm{Ly}\alpha} \approx 3.66$ for a b parameter of $26\,\mathrm{km\,s}^{-1}$) and the latter for optically thick absorbers ($N_{\mathrm{HI}} > 10^{17.2}\,\mathrm{cm}^{-2}$).

Figure 5.2 shows the covering fractions of gas with different Lyα absorption strength, within a given distance bin from the centers of haloes with $M_{\mathrm{h}} > 10^{11.5}\,\mathrm{M}_{\odot}$. The maximum optical depth is measured within $165\,\mathrm{km\,s}^{-1}$ from galaxy positions. Rakic et al. (2011) found that the signal is independent of velocity within $165\,\mathrm{km\,s}^{-1}$, and that the errors are strongly correlated for smaller velocity differences, so they chose this velocity interval for many of their calculations. We use the same interval here to facilitate the comparison with their observations. We note that this velocity interval is larger than the estimated galaxy redshift errors in the observations ($\sigma = 125\,\mathrm{km\,s}^{-1}$). On the other hand, the column density results are based on the total column density along the LOS through the 50 h^{-1}cMpc box. We use such projections only for optically thick absorbers, and since they are relatively rare, they will likely reside in the vicinity of galaxies (the maximum impact parameter here is 200 pkpc). Also, it is unlikely that a collection of weak absorbers along the LOS could cumulatively account for such large column densities (see Altay et al. 2011). We use a total column density along the LOS for practical reasons, as finding column densities for individual absorbers would require decomposing the spectra into Voigt profiles, which is impractical for the number of sightlines considered here. We verified that this is a good approximation for e.g. LLSs, where we found the expected maximum optical depth of an absorber with LLS column densities (assuming a b parameter of $26\,\mathrm{km\,s}^{-1}$), and performed the analysis equivalent to the one we apply to optically thin absorbers, and found almost perfect agreement with results based on the to-

tal column density along the LOS. Naturally, redshift errors have no effect on such estimated column density results.

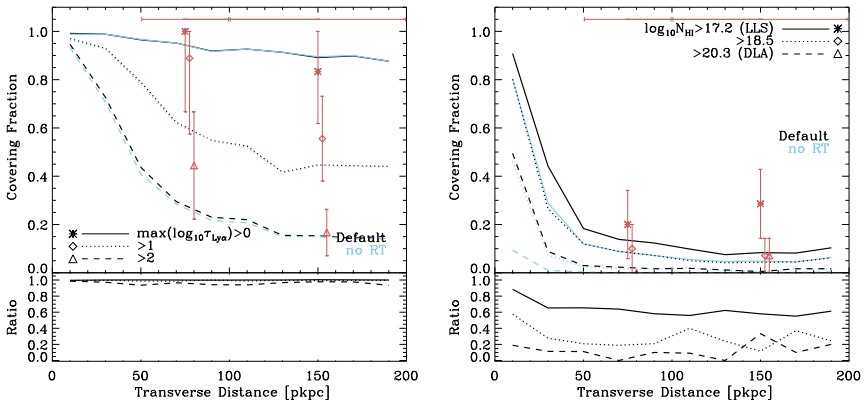

Figure 5.2 – *Top panels*: covering fractions of absorbers with maximum H I Lyα optical depth $\log_{10}\tau_{\mathrm{Ly}\alpha} > 0$, 1, 2 (left panel), and covering fractions of absorbers with $\log_{10}N_{\mathrm{HI}} \geq$ 17.2 (LLSs), 18.5, and 20.3 cm^{-2} (DLAs) (right panel), as a function of impact parameter from the center of haloes with $M_{\mathrm{h}} > 10^{11.5}$ M$_{\odot}$ at z=2.25. Black lines show the results for the default case, i.e. absorption from all gas, in the simulation with radiative transfer applied in post-processing. The blue lines show the results for the simulation without radiative transfer, which fall on top of the black curves in the left panel (radiative transfer does not make a difference for gas optically thin to ionizing radiation). The red symbols show the covering fractions observed by Rakic et al. (2011) in the left panel, and by Rudie et al. (in prep.) in the right panel. The covering fractions are measured in 20 pkpc bins for the simulations, and in 100 pkpc bins for the observations (top horizontal bars show the extent of the bins for the observations, where the first bin effectively starts only at 55 pkpc, which is equal to the smallest impact parameter). *Bottom panels:* the ratios between the blue and black curves, i.e. the effect of the radiative transfer.

The left panel of Figure 5.2 shows the covering fraction of sightlines with gas with maximum H I Lyα optical depth higher than 1, 10, or a 100, within $\pm 165\,\mathrm{km\,s^{-1}}$ of a halo of mass $M_{\mathrm{h}} > 10^{11.5}$ M$_{\odot}$ at $z = 2.25$, while the right panel shows the same but for gas with the H I column densities greater than $10^{17.2}$, $10^{18.5}$, and $10^{20.3}\,\mathrm{cm^{-2}}$. The blue lines show the results for the simulation that was not treated with radiative transfer, and the black lines for the case where it was applied in post-processing. As expected, the radiative transfer does not affect the results significantly for absorbers optically thin to the ionizing radiation (left panel). Although this panel includes all absorbers with optical depth higher than a given value from the optically thin regime, i.e. also absorbers that are optically thick, strong absorbers are relatively rare and the covering fraction is dominated by weaker absorbers. In the discussion below we will refer to absorbers from the left panel as 'optically thin', even though they include optically thick absorbers as well. However, the situation is dramatically different for optically thick absorbers, as can be seen in the

right panel. Without radiative transfer the covering fraction of DLAs is ~ 5 times smaller. This demonstrates the importance of this post-processing step for studying high column density absorbers close to galaxies.

The covering fraction of absorbers with maximum $\tau_{\mathrm{Ly}\alpha} \geq 1$, 10, and 100, changes from unity within 20 pkpc to ≈ 0.90, ≈ 0.45, and ≈ 0.15, respectively, at an impact parameter of 200 pkpc. The covering fraction of optically thick absorbers changes from ~ 0.90 (~ 0.45) for LLSs (DLAs) within 20 pkpc, to ~ 0.15 (~ 0.02) at 200 pkpc. Below we will refer to the covering fraction for the default case (i.e. all gas) as the "total covering fraction".

In the same figure we also show covering fractions of absorbers measured from observations. In the left panel (for the optically thin lower limit) we show the covering fractions measured by Rakic et al. (2011), and in the right panel (for the optically thick regime) we use the results from Rudie et al. (in preparation). These covering fractions were estimated in two bins of 100 pkpc, as compared to 20 pkpc for the simulated data. The observed covering fractions should therefore be compared to the simulated ones by averaging simulated covering fractions over appropriate distances. In addition, the smallest impact parameter in the observations is ≈ 55 pkpc, which should also be taken into account for the comparison. It appears that the simulations match all observed covering fractions, except that for $N_{\mathrm{HI}} > 10^{17.2}\,\mathrm{cm}^{-2}$ from 100 to 200 pkpc, although the errors on the observations are large. Given that Rudie et al. (2011) observe only 1 absorber with $N_{\mathrm{HI}} > 10^{18.5}\mathrm{cm}^{-2}$ in each 100 pkpc bin, we will not use (dis)agreement with observations in the optically thick regime to determine the importance of cold-mode gas for the total covering fraction of Lyα absorbers.

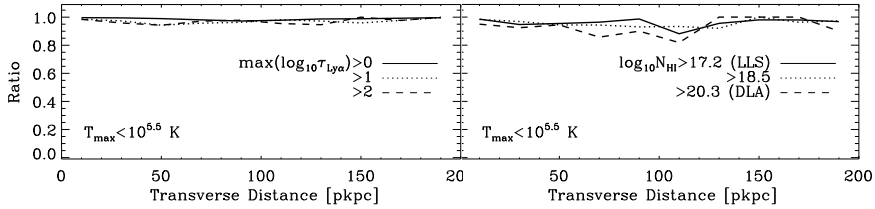

Figure 5.3 – The ratios of covering fractions of absorbers with a given minimum absorption strength including only gas with the maximum past temperature of $\lesssim 10^{5.5}$ K and total covering fractions (i.e. absorption from all gas), as a function of impact parameter. *Left panel* shows the ratios for absorbers with maximum H I Lyα optical depth $\log_{10}\tau_{\mathrm{Ly}\alpha} \geq 0$, 1, and 2. *Right panel:* similar to the left panel, but for optically thick absorbers with $\log_{10}N_{\mathrm{HI}} \geq 17.2$ (LLSs), 18.5, and 20.3 cm^{-2} (DLAs).

Figure 5.3 shows the fractional contribution that gas with a maximum past temperature $\lesssim 10^{5.5}$ K makes to the total covering fraction within 200 pkpc from galaxy haloes, for both optically thin and optically thick absorbers. The covering fraction of such gas is equal to the value on the y-axis multiplied by the covering fraction in Figure 5.2 (black lines). We note that the results

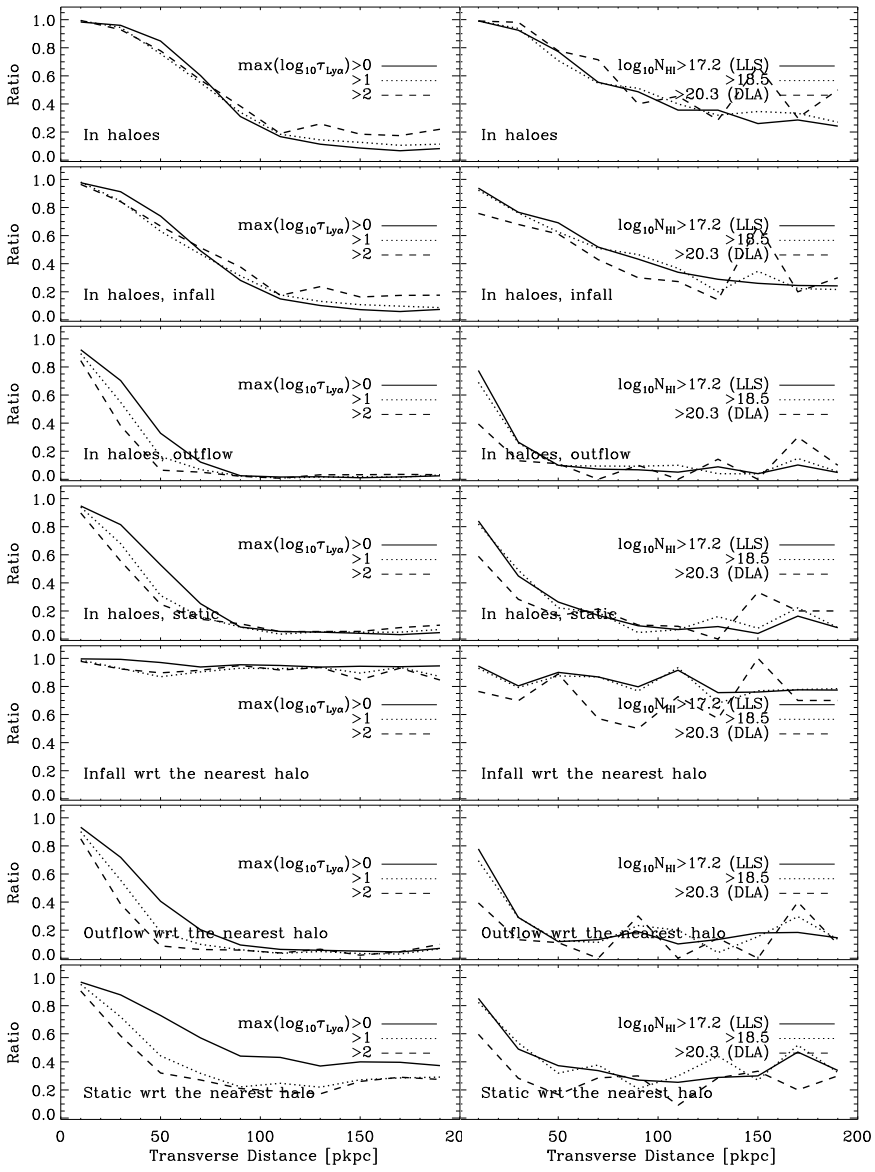

Figure 5.4 – Similar to Figure 5.3, but for more cuts referring to the gas halo membership (in haloes with $M_{\rm h} > 10^{11.5}$ M$_\odot$) and kinematics with respect to the nearest halo with $M_{\rm h} > 10^{11.5}$ M$_\odot$ (in units of $R_{\rm vir}$) at velocities $v > 0.25 v_{\rm circ}$ for inflowing and outflowing gas, and $v < 0.25 v_{\rm circ}$ for static gas.

are noisy for DLAs, due to small number statistics. The covering fraction of DLAs at distances $\gtrsim 50$ pkpc is only a few per cent (Figure 5.2) which means

that an estimate in any given 20 pkpc distance bin (with ≈ 200 sightlines per bin) is based on only a few DLAs.

Gas with a maximum past temperature $\lesssim 10^{5.5}$ K has a covering fraction that is almost identical to the total covering fraction. Given that these covering fractions are consistent with the observations, it appears that cold-mode gas can account for Lyα absorption near galaxies from Rakic et al. (2011) and Rudie et al. (2011, in preparation).

We next determine how much absorption near haloes with $M_{\rm h} > 10^{11.5}{\rm M}_{\odot}$ comes from gas within those haloes. We select all the particles belonging to haloes with $M_{\rm min} = 10^{11.5}\,{\rm M}_{\odot}$. It is likely that some of the haloes in this mass range overlap, and that by studying the distribution near one such halo, we also intersect absorption by gas belonging to a different halo. We expect the contribution from neighboring halos to be small, and leave the precise treatment of this issue for future work.

Figure 5.4 shows that for impact parameters $\lesssim 30$ pkpc, gas in haloes produces a covering fraction that is almost identical to the total for absorbers of all strengths. At larger distances, the contribution of haloes asymptotes to $\sim 10\%$ of the total for gas with $\tau_{{\rm Ly}\alpha} \geq 1$, and to $\sim 25\%$ of the total for optically thick absorbers. This suggests that optically thick gas is more likely to reside in the halo. Van de Voort et al. (2011c) also found that the likelihood of halo membership increases with the strength of Lyα absorption. We also see that the probability of optically thick systems belonging to the halo in question declines with distance. We investigated (not shown here) the origin of the remainder of optically thick absorbers that contribute to the total covering fraction and found that they reside within smaller haloes. By multiplying the curves in the top left panel of Figure 5.4 with the corresponding covering fractions in Figure 5.2 (black lines), we conclude that gas in haloes with $M_{\rm h} > 10^{11.5}\,{\rm M}_{\odot}$ cannot account for the observed covering fractions. We cannot draw any conclusions about the optically thick gas due to small number statistics.

Gas within the haloes that is moving towards their centers with a radial velocity greater than 1/4 of the halo circular velocity, $v_{\rm circ} = \sqrt{GM_{\rm vir}/R_{\rm vir}}$, has a covering fraction that is similar to that of all gas that is in haloes (second set of panels from the top). We take a threshold value of 1/4 of the circular velocity because the contribution of gas that is moving at velocities higher than the circular velocity is negligible. Gas that is outflowing with $v > 0.25v_{\rm circ}$ and gas that is "static" with respect to the halo center (i.e. $v < 0.25v_{\rm circ}$), generally has a lower covering fraction than the inflowing gas. The covering fractions of outflowing and static gas are similar, and for optically thin (thick) gas they change from $\sim 90\%$ ($\sim 80\%$) of the total covering fraction within 20 pkpc, to $\sim 5\%$ ($\sim 10\%$) at 200 pkpc.

If we relax the condition about halo membership, and instead only consider whether the gas is falling towards the nearest halo with $M_{\rm h} > 10^{11.5}{\rm M}_{\odot}$

with a velocity greater than a quarter of the circular velocity of that halo, we find that the covering fraction of such gas is $\gtrsim 85\%$ of the total within 200 pkpc for optically thin gas. This shows that most of the Lyα absorbing gas is accreting onto the haloes, even though it is not yet inside them. The covering fraction of this gas is consistent with the observations, which suggests that (if the *REF* model describes reality sufficiently well) the infalling gas is necessary to account for the observed covering fraction within 200 pkpc. The covering fraction of optically thick absorbers is $\lesssim 20\%$ lower than total at all distances, suggesting that most strong absorbers (and their small haloes) are moving towards larger haloes. Gas that is moving away from the nearest massive halo with $v > 0.25 v_{\rm circ}$, as well as static gas (i.e. $v < 0.25 v_{\rm circ}$), has a covering fraction that is $\lesssim 20\%$ and $\lesssim 40\%$, respectively, of the total at distances $\sim 50 - 200$ pkpc, and therefore also comprises a significant amount of gas. Their covering fractions alone are insufficient to account for the observations.

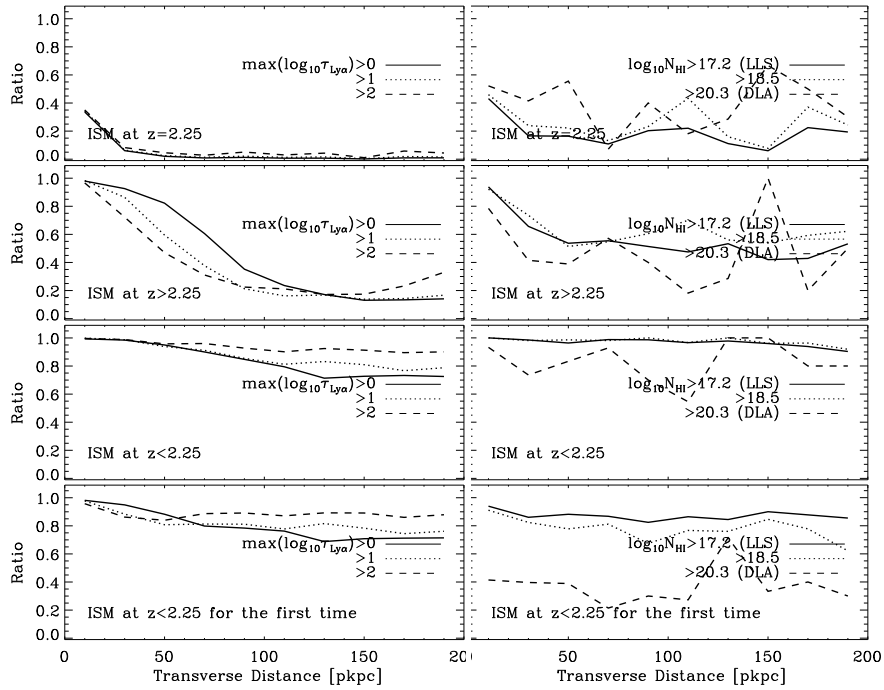

Figure 5.5 – Similar to Figure 5.3, but for more cuts referring to the gas participation in the ISM of galaxies, before, at, and after $z = 2.25$.

Figure 5.5 refers to the gas past, present, and future participation in the ISM of galaxies, which we define as any gas with density $n_{\rm H} \geq 0.1\,{\rm cm}^{-3}$ (see §5.2.2). The contribution of the ISM to the covering fraction of Lyα absorbing gas increases closer to the centers of haloes and with increasing absorption

strength. Within 200 pkpc, $\sim 20-40\%$ of optically thick absorbers are part of the ISM. At 200 pkpc, however, we do not expect them to be the ISM of the central galaxy, but of companion galaxies.

Gas that was part of the ISM at $z > 2.25$, but is not in the ISM at $z = 2.25$, has a covering fraction close to the total within 20 pkpc, and then it asymptotes to $\sim 20\%$ ($\sim 60\%$) of the total covering fraction at 200 pkpc for optically thin (thick) gas. Gas that will become part of the ISM at $z < 2.25$, but is not ISM at $z = 2.25$, has a covering fraction $\gtrsim 80\%$ ($\gtrsim 90\%$) of the total for optically thin (thick) gas within 200 pkpc, and most of that gas will accrete onto a galaxy for the first time. The covering fraction of this gas is consistent with the observations for maximum $\log_{10}\tau_{\mathrm{Ly}\alpha} > 0$ and > 2, but is lower than observed for maximum $\log_{10}\tau_{\mathrm{Ly}\alpha} > 1$ (1σ discrepancy). This suggests that gas that will become the ISM of galaxies by $z = 0$ can be observed in absorption at $z \approx 2.4$. Gas that accretes onto a galaxy after $z = 2.25$ but not for the first time, is the "recycled" gas (Oppenheimer et al. 2010). This is gas that was in the ISM before $z = 2.25$, and then for example got stripped or ejected from the ISM through outflows, but accretes again onto galaxies at $z < 2.25$. In addition, stronger absorbers are more likely to become the ISM of galaxies than weaker absorbers at the same separation from haloes, as can be seen by comparing the left and right panels.

We note that in order to say with certainty whether any of the gas samples is crucial for the observed absorption, it would be necessary to consider absorption by all but gas in a given sample (e.g. all but gas with $T_{\mathrm{max}} < 10^{5.5}$ K). If it turns out that the predicted absorption in such gas is insufficient to account for the observations, we can conclude that that gas sample (e.g. cold-mode gas) plays a major role and had been observed already. Also, it is necessary to determine how sensitive the results are to different feedback prescriptions. We leave treatment of these issues for our future publication.

5.4 Absorption by cold flows on pMpc scales

In the previous Section we considered the distribution of H I around galaxies on scales that are comparable to the sizes of the dark matter haloes hosting the galaxies used in Rakic et al. (2011), i.e. < 200 pkpc, $\lesssim 2R_{\mathrm{vir}}$. In this section we will study H I Lyα absorption as a function of distance from the galaxies on scales up to 5 pMpc ($\gg R_{\mathrm{vir}}$) by analyzing the median optical depth as a function of 3-D Hubble distance from haloes. This distance is equal to $\sqrt{d_{\mathrm{LOS}}^2 + b^2}$, where d_{LOS} is the LOS separation between the halo and the absorber estimated from their velocity separation assuming that it is due to Hubble expansion, and b is the impact parameter. We will compare the simulated absorption distributions with the observations of Rakic et al. (2011), and therefore we set the minimum impact parameter in the simulations to match their observations, i.e. to 55 pkpc.

Figure 5.6 shows the effect of the improved handling of radiative transfer

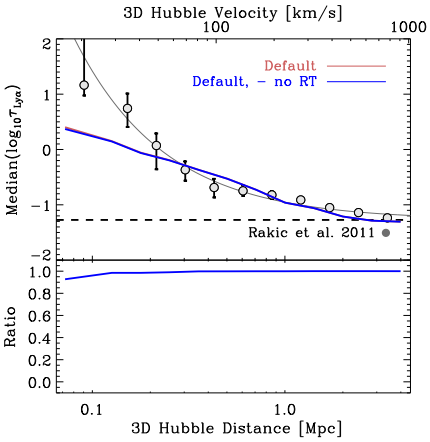

Figure 5.6 – *The Top panel* shows the median $\log_{10}(\tau_{\mathrm{Ly}\alpha})$ as a function of physical 3-D Hubble distance from galaxy halos. The circles show the observed points with 1σ error bars from Rakic et al. (2011), the red curve shows the results obtained from simulations where self-shielding was applied in post-processing, and the blue curve shows the case where we apply no self-shielding correction. *The lower panel* shows the ratio of the latter and former. Self-shielding makes negligible difference to the median level of absorption at distances greater than 200 pkpc from galaxies, and $\sim$ 10% difference for distances $\lesssim$ 100 pkpc.

on absorption at large distances from galaxies. Without applying self shielding in post-processing, the median level of absorption within $\sim 55-100$ pkpc from galaxies is $\sim$ 10% lower, while at larger distances it is nearly identical to the case with radiative transfer. This is consistent with Figure 5.2, which showed that radiative transfer does not change the results for optically thin absorbers, and far away from galaxies we expect gas to be predominantly optically thin. The simulation under-predicts the absorption level within $\sim$ 200 pkpc from galaxies in comparison with the observations from Rakic et al. (2011). This is probably due to cold gas physics in the simulations not being captured sufficiently well (e.g. in reality gas at ISM densities can self-shield to form a cold phase with $T \ll 10^4$ K, while in the simulations its temperature stays at $\gtrsim 10^4$ K), as well as potentially not fully adequate SN feedback prescription in the *REF* model (as we will show below, feedback can raise gas temperature close to haloes).

The top left panel of Figure 5.7 shows that if we only include gas that was never heated to temperatures $T > 10^{5.5}$ K, then the absorption level decreases by $\approx$ 20% within $\approx$ 130 pkpc from galaxies, and by only $\lesssim$ 5% at distances $\gtrsim$ 1 pMpc. In other words, gas that was never heated to $T > 10^{5.5}$ K accounts for almost all absorption in the Lyα forest, and only close to galaxies is there a mixture of hotter gas that cooled down sufficiently to absorb in H I Lyα and gas that is considered to be part of cold accretion. At distances $\gtrsim$ 200 pkpc, the absorption profile of gas with $T_{\mathrm{max}} < 10^{5.5}$ K is consistent

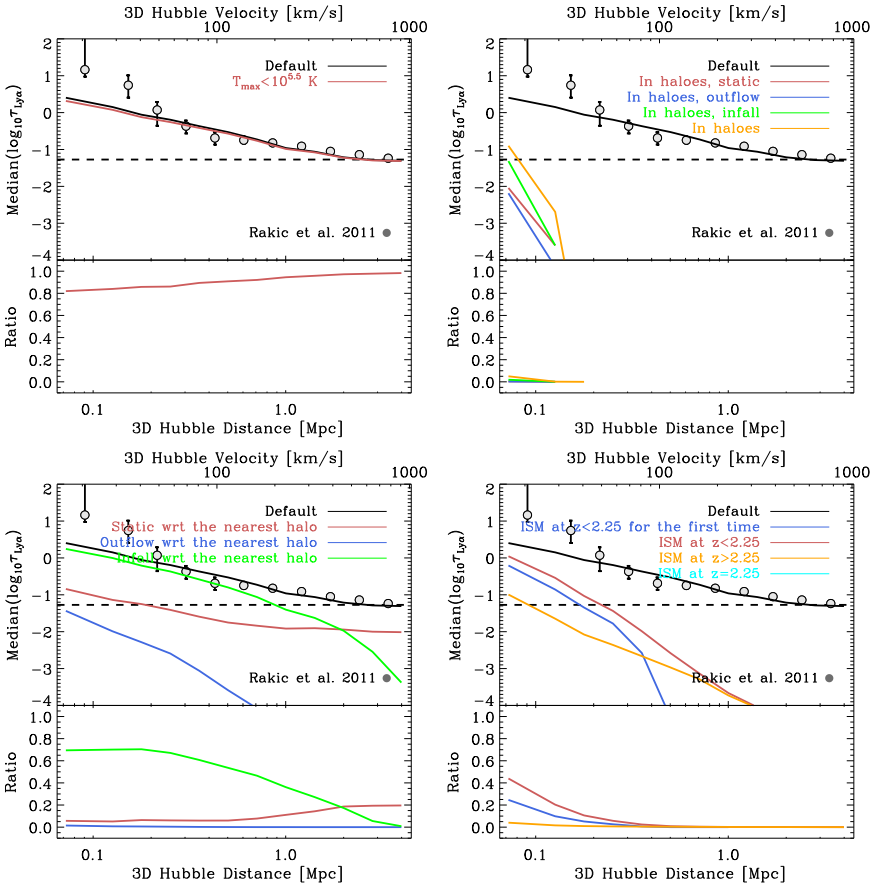

Figure 5.7 – *The top parts of all panels* show the median $\log_{10}(\tau_{\rm Ly\alpha})$ as a function of physical 3-D Hubble distance from $M_{\rm h} > 10^{11.5}\,{\rm M}_{\odot}$ galaxy halos at $z = 2.25$, where colored curves represent results when different gas samples are included, as indicated in the legends. *The bottom parts of all panels* show the ratios between the curves for different cuts and the default curve. The dashed line shows the median optical depth of all pixels. *The top right panel* shows the median optical depth of gas that is in haloes with $M_{\rm h} > 10^{11.5}\,{\rm M}_{\odot}$, and also of gas that is in addition moving with respect to the halo center with radial velocities $v > 0.25 v_{\rm circ}$ (for infalling and outflowing gas) and $v < 0.25 v_{\rm circ}$ (static gas).

with the observed profile. A comparison with Figure 5.2, which showed that within 200 pkpc the covering fraction of gas with $T_{\rm max} < 10^{5.5}\,{\rm K}$ is almost identical to the total covering fraction, shows that the effect on the median absorption statistics is larger.

In the top right panel of Figure 5.7 we apply more stringent cuts. It appears that gas that is within the host haloes produces absorption that is $\gtrsim 90\%$ smaller than the total absorption within ≈ 130 pkpc from the galaxies,

while at distances $\gtrsim 130$ pkpc its contribution is negligible. This is consistent with results from the previous Section (5.3), where strong absorbers are confined to haloes, and lower optical depth gas is less likely to be in haloes, which is why contribution of halo gas is negligible at large distances. Considering that 130 pkpc is comparable to the $R_{\rm vir}$ of the haloes, and that halo gas produces very small median optical depth within that 3-D distance, suggests that gas that is outside haloes, but due to peculiar velocities absorbs at halo positions, is a very important contributor.

Halo gas that is moving towards the halo center with $v > 0.25v_{\rm circ}$ produces absorption that is only a few percent of the total within 130 pkpc, and negligible beyond. Outflowing and static gas produce even weaker absorption.

In the bottom left panel of Figure 5.7 we see that if we include all gas that is moving towards the nearest halo (with $M_{\rm min} = 10^{11.5}$ M$_\odot$) with $v > 0.25v_{\rm circ}$ (where $v_{\rm circ}$ is the circular velocity of that halo) rather than only the gas within the haloes, then such gas makes a significant contribution to absorption even far from galaxies. This reflects the ongoing structure formation in the Universe where even low-density gas is undergoing motion towards large-scale overdensities. It produces absorption that is $\sim 30\%$ lower than the total within ~ 0.5 pMpc, and then slowly falls off to being only a few percent of the total at 5 pMpc. Gas that is going away from the galaxies with $v > 0.25v_{\rm circ}$ produces a median absorption level that is $\lesssim 1.5\%$ of the total at all distances from galaxies. Gas that is static relative to the galaxies ($v < 0.25v_{\rm circ}$) produces absorption that is $\lesssim 10\%$ of the total within ~ 1 pMpc from galaxies, but its contribution grows to $\sim 20\%$ of the total at ~ 5 pMpc, where it also surpasses the absorption by inflowing gas. The picture on large scales is quite different from that within 200 pkpc of the galaxies, where the covering fractions of outflowing and static gas are comparable. This suggests that outflowing gas becomes less important further away from galaxies.

In the bottom right panel of Figure 5.7 we select gas that is part of the ISM at $z = 2.25$, at $z > 2.25$, $z < 2.25$, and at $z < 2.25$ for the first time. The ISM contributes a negligible amount of Lyα absorption on the distance scales considered, and its median optical depth is consistent with zero. Absorption by ejected gas, i.e. gas that has been in galaxies before and is not at $z = 2.25$, is $\sim 95\%$ lower than total absorption within ≈ 130 pkpc from galaxies, and its contribution is negligible beyond that distance. Gas that is not in the ISM at $z = 2.25$, but becomes part of it after that redshift, produces significant absorption out to ~ 0.5 pMpc, and its median optical depth is only $\sim 50\%$ lower than total within ~ 130 pkpc from the galaxies. Most of this gas becomes the ISM after $z = 2.25$ for the first time. An interesting result from this panel is that although gas that is closer to galaxies is more likely to join the ISM, most of the Lyα absorbing gas at distances greater than ~ 200 pkpc will not accrete onto the galaxy before $z = 0$.

5.5 Physical properties of the Lyman-α absorbing gas

In this section we show the physical properties of the H I Lyα absorbing gas in the simulations. Given that the predicted median absorption profiles do not exactly match the observations, the relations below might not resemble the true gas densities and temperatures in those regions. However, we consider them useful for building intuition about gas properties, especially farther away from galaxies where the absorption profiles between observations and simulations agree well. We also note that the simulations used below were not post-processed with radiative transfer, unlike all previous results presented in this chapter.

In the figures below we show three different overdensity and temperature profiles of gas as a function of 3-D Hubble distance from the haloes:

i) mass weighted, in real space;
ii) $N_{\rm HI}$ weighted, i.e. weighted by the contribution to the optical depth, in real space;
iii) optical depth weighted, i.e. weighted by the contribution to the optical depth of the pixel. This estimate is almost identical to the $N_{\rm HI}$ weighted one, the only difference being that it is evaluated in velocity space.

Along each sightline used in the previous section, we extract gas density and temperature distributions (that were used for calculating absorption spectra in the first place). Estimates of these quantities in real space were extracted from the simulations by ignoring peculiar velocities, as opposed to those estimated in velocity (i.e. redshift) space. We estimate the profiles below as a function of 3-D distance, where for quantities extracted in redshift space (i.e. the optical depth weighted overdensity and temperature) we assume that the LOS separation between haloes and pixels is due only to the Hubble flow.

Figure 5.8 compares the different median overdensity profiles, for the halo mass range of interest. The $N_{\rm HI}$ weighted overdensity is higher than the mass weighted overdensity suggesting that Lyα absorbing gas is denser than the gas that makes up most of the mass. The optical depth weighted overdensity profile, which only differs from the $N_{\rm HI}$ profile in that it is estimated in redshift space, is also higher than the mass weighted profile. In comparison with the $N_{\rm HI}$ profile, however, it shows a shallower slope with distance, because it is affected by the peculiar motions of the gas. The median optical depth weighted overdensity also appears higher than the median $N_{\rm HI}$ weighted overdensity, which is due to overdense absorbers having relatively small sizes in real space that get smoothed in redshift space due to peculiar velocities. For example, Lyα absorbers with the column density $N_{\rm HI} = 10^{16}\,{\rm cm}^{-2}$ have typical sizes of ~ 20 pkpc (Schaye 2001), while the typical Doppler parameter of such absorbers is $\approx 30\,{\rm km\,s}^{-1}$ (Rudie et al. 2011, in preparation) making them smeared over $\gtrsim 100$ pkpc in redshift space at $z = 2.25$.

The left panel of Figure 5.9 shows the different median temperature pro-

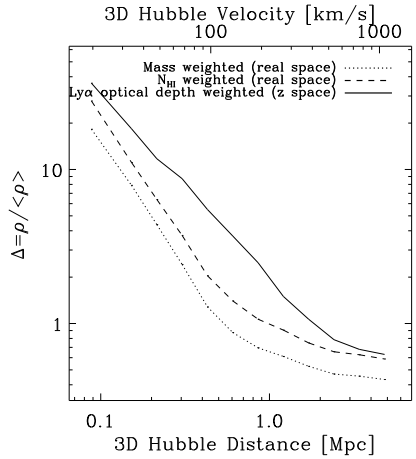

Figure 5.8 – Mass weighted (dotted lines), $N_{\rm HI}$ weighted (dashed lines), and H I Lyα optical depth weighted (solid lines) median overdensity of gas as a function of distance from the haloes, with mass $\rm M_h > 10^{11.5}\,M_\odot$ at $z = 2.25$, in the 50 h^{-1} cMpc *REF* simulation.

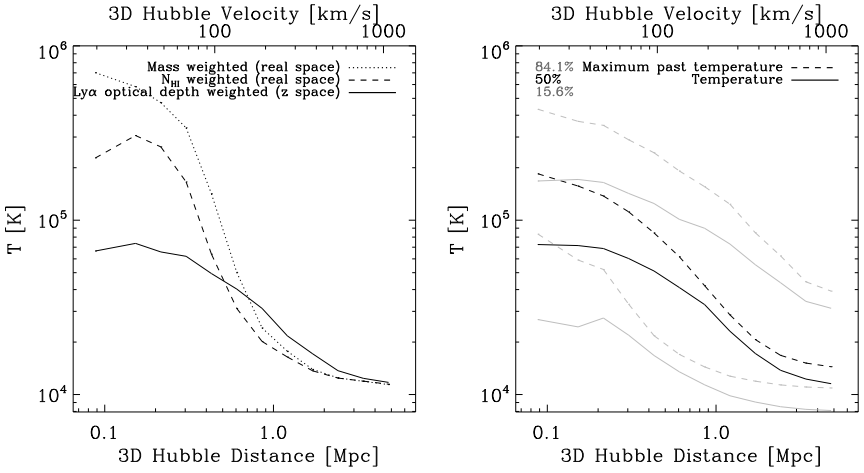

Figure 5.9 – The left panel shows the median mass weighted (dotted lines), $N_{\rm HI}$ weighted (dashed lines), and H I Lyα optical depth weighted (solid lines), temperatures as a function of distance from the haloes, with $\rm M_h > 10^{11.5}\ M_\odot$ at $z = 2.25$, in the 50 h^{-1} cMpc *REF* simulation. In the right panel we repeat the optical depth weighted median temperature of the gas from the left panel (black solid line) and show also the median of the maximum temperature that the Lyα absorbing gas has ever reached (black dashed line). Grey lines show the corresponding 15.1 and 84.1 percentiles (encompassing the 1σ interval around the median).

files. The mass weighted temperature is higher than the $N_{\rm HI}$ weighted temperature, because it traces all gas, including gas that is collisionally ionized

at the virial temperature ($T_{\rm vir} > 10^{5.5}$ K). The Lyα absorption traces denser and colder, neutral gas. The optical depth weighted temperature is also lower than the mass weighted temperature, and the profile is shallower than the $N_{\rm HI}$ weighted temperature due to peculiar velocities. The optical depth weighted temperature is lower than the ion weighted temperature in the innermost regions because peculiar velocities bring the colder gas closer to galaxy redshifts in velocity space (see Chapter 4 where we found that neglecting peculiar velocities reduces the signal close to galaxies).

The right panel of Figure 5.9 compares the median optical depth weighted current gas temperature with the median optical depth weighted maximum temperature that the gas has ever reached, as a function of distance from the halo. The 1σ scatter around the median is also shown. Most of the Lyα absorbing gas is and has always been cold ($\rm T_{max} \lesssim 10^{5.5}$ K), while there is a mixture of hot- and cold-mode gas close to galaxies ($\lesssim 200$ kpc). This is consistent with the findings presented in the previous two sections.

Each panel of Figure 5.10 shows the median optical depth weighted overdensity and temperature of gas as a function of the optical depth for a particular range of impact parameters (estimated over $\pm 165\,{\rm km\,s^{-1}}$ along the LOS from galaxy positions), in the *REF* model. In each panel we also show the results for 1000 random sightlines (grey lines), which is identical in each panel. Looking at the results for random sightlines, we notice that both the overdensity and the temperature increase with the optical depth, for $-2 \lesssim \log_{10}\tau \lesssim 1$. This reflects the well-known temperature-density relation (e.g. Hui & Gnedin 1997), where the temperature of the IGM is set by the competition between adiabatic cooling due to the expansion of the Universe and photoheating. At the low optical depth end ($\log_{10}\tau_{\rm Ly\alpha} < -2$) there is an upturn in both the density and temperature due to gas that is shock-heated to high temperatures and therefore highly ionized. At the high optical depth end ($\log_{10}\tau_{\rm Ly\alpha} > 1$) the temperature decreases with increasing optical depth and density, because this gas is dense enough to cool radiatively.

Even for impact parameters $1.42 < b < 2$ pMpc the temperature for a given optical depth in the range $-1 \lesssim \log_{10}\tau \lesssim 1$ is higher than for a random sightline. Approaching galaxies, the temperature of the Lyα absorbing gas increases further and for $b \lesssim 0.5$ pMpc the density corresponding to a fixed optical depth also becomes noticeably higher than for a random place. The temperature-density relation (for $-2 \lesssim \log_{10}\tau \lesssim 1$) gets gradually inverted with decreasing impact parameter and is almost fully inverted at $b \lesssim 0.25$ pMpc; instead of both gas temperature and overdensity increasing with optical depth, the temperature is higher for low optical depths. Absorbers with optical depth $\tau = 0.1$ are gas clouds with a typical overdensity of $\sim 1-2$ and a temperature $T \sim 2 \times 10^4$ K at ~ 2 Mpc from galaxies, but they are gas clouds with overdensity ~ 10 and temperature $\sim 10^5$ K within ~ 100 pkpc from galaxies. This means that *gas with the same Lyα optical depth has very different properties depending on where it is with respect to the haloes.*

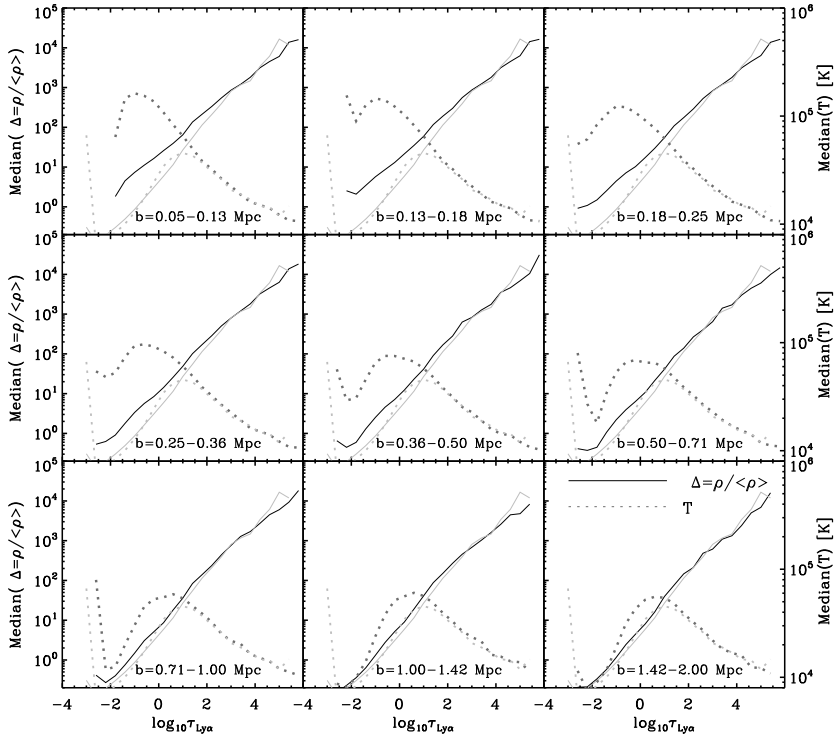

Figure 5.10 – Different panels show the $z = 2.25$ median H I Lyα optical depth weighted overdensity (solid black line, left axis) and temperature (dotted black line, right axis) as a function of the optical depth, with different impact parameter ranges shown in different panels (estimated over $\pm 165\,\mathrm{km\,s^{-1}}$ from halos with $M_\mathrm{h} > 10^{11.5}\,\mathrm{M}_\odot$). The grey lines are repeated in each panel and show the results for sightlines drawn at random positions. We can see that gas with the same optical depth has very different properties depending on where it is with respect to the haloes.

Figure 5.11 is similar to Figure 5.10 but shows the properties of absorbers with a given optical depth for the *AGN* model. With respect to the *REF* model (grey curves), more gas has been shock-heated to high temperatures at the low optical depth end, and the temperature-density relation is already fully inverted at impact parameters $b \lesssim 1$ pMpc.

In Figure 5.12, we show the results for the *NOSN* model. Comparing them with results for the *REF* model (grey curves), it becomes obvious that at least some of the temperature-density inversion, for $-2 \lesssim \log_{10}\tau \lesssim 1$, at small impact parameters is due to SN feedback. Nevertheless, even pure gravitational heating is able to somewhat invert the temperature-density relation.

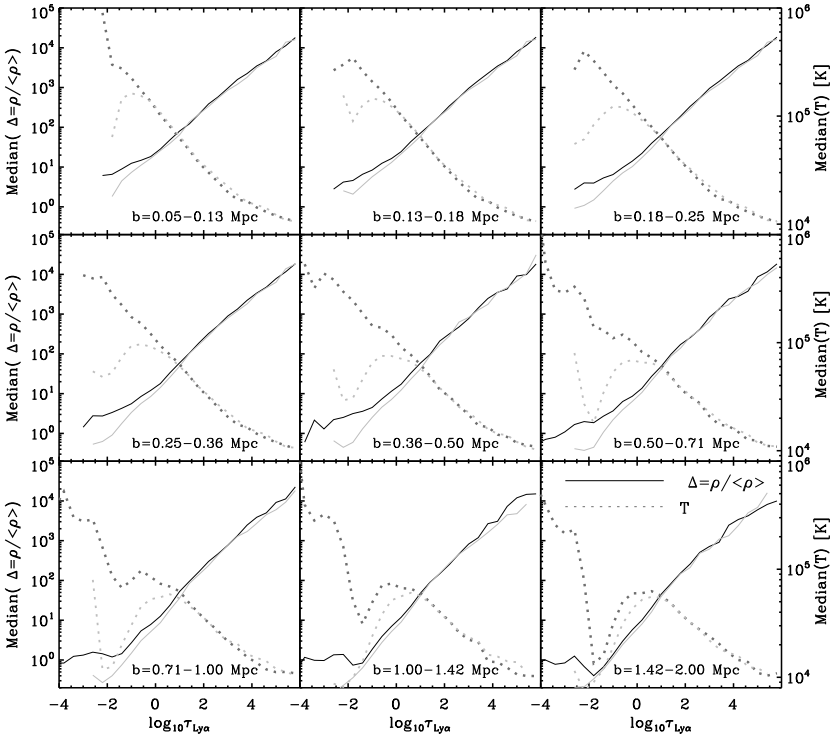

Figure 5.11 – Similar to Figure 5.10 but for the *AGN* model. The grey lines show the results for the *REF* model. In comparison with the *REF* model, gas properties are affected at greater distances from the galaxies.

5.6 Summary & Conclusions

Cold flows are thought to be the dominant process through which galaxies acquire fuel for star-formation, but there is no unequivocal observational evidence for their existence as of yet. Here we explore how much of the gas seen in H I Lyα absorption at $z = 2.25$ is due to cold flows. We use the reference model from the OWLS suite of simulations (Schaye et al. 2010), with radiative transfer applied in post-processing, and study absorption near haloes with $M_{\rm h} \geq 10^{11.5}\,{\rm M}_{\odot}$, which are expected to host the galaxies from Rakic et al. (2011). Our results are dominated by haloes with $M_{\rm h} \sim 10^{12}\,{\rm M}_{\odot}$, which is where the simulations predict that the cold and hot modes provide comparable contributions to the gas accretion rates onto haloes (Van de Voort et al. 2011a). We found that the improved radiation transfer handling is only important for the part where we focus on the dense halo gas which can self-shield against the ionizing radiation.

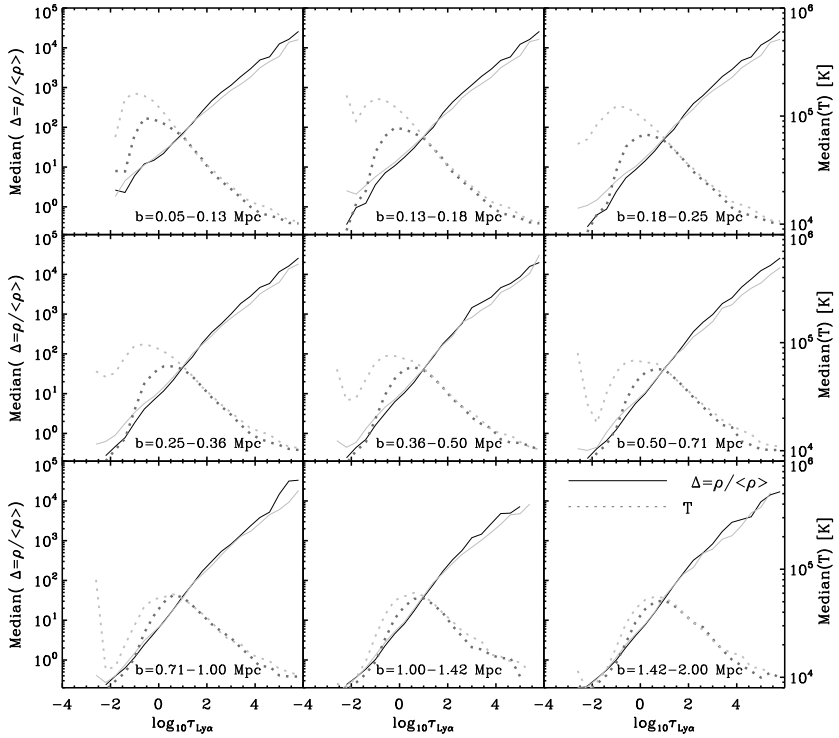

Figure 5.12 – Similar to Figure 5.10, but for the *NOSN* model. In comparison with the *REF* model (grey curves), the temperature density-relation is less inverted at small impact parameters, suggesting that at least some of the heating is due to SN-driven winds.

In the first part of this chapter we studied the nature of the Lyα absorbing gas by examining its past and future properties, and in the second part we studied its temperature and density. We looked into their dependence on the feedback implementation by using simulations with SN feedback (the reference model), with both SN and AGN feedback (model *AGN*), and without feedback (model *NOSN*). Unlike in the first part of the chapter, radiative transfer was not applied to any of these simulations.

We studied the covering fraction of absorbers with a given strength in the immediate surroundings of the halo, i.e. at impact parameters $b \leq 200$ pkpc, as a function of impact parameter, and across $\pm 165\,\mathrm{km\,s^{-1}}$, for gas that is optically thin to the ionizing radiation. For gas with column densities $N_{\mathrm{HI}} \geq 10^{17.2}\,\mathrm{cm^{-2}}$ we instead considered the total column density along the sightline through the simulation volume. We compared the predicted covering fractions to those observed by Rakic et al. (2011) for maximum $\log_{10}\tau_{\mathrm{Ly}\alpha} > 0$, 1, and 2, and Rudie et al. (2011, in preparation) for $\log_{10}N_{\mathrm{HI}} > 17.2$, 18.5,

and 20.3 cm^{-2}. We found that:

- Most of the Lyα absorbing gas within 200 pkpc from galaxies has not been shock heated to temperatures $T > 10^{5.5}$ K.
- Gas is mostly moving towards the haloes with $v > 0.25 v_{\rm circ}$, although a non-negligible fraction is flowing outwards (also with $v > 0.25 v_{\rm circ}$), or is static with respect to the halo centers (i.e. $v < 0.25 v_{\rm circ}$).
- Most of the Lyα absorbing gas is on its way to joining the ISM of galaxies after the time of observation ($z = 2.25$), and will be accreting for the first time. Optically thick gas is more likely to become part of galaxies before $z = 0$ than weaker absorbers at the same impact parameter.
- Gas with $T_{\rm max} \lesssim 10^{5.5}$ K has a covering fraction that is consistent with the observed covering fraction of gas with maximum $\log_{10}\tau_{\rm Ly\alpha} > 0$, 1, and 2. Gas that is infalling towards haloes, but is not necessarily inside them, and gas that will join the ISM of galaxies by $z = 0$, also have covering fractions that are consistent with the observed.

In order to say whether different gas samples have a critical role in accounting for the observed covering fraction, it would be more appropriate to exclude particles belonging to those samples, and compare the absorption produced by the remaining gas to the observed absorption. If the remaining gas exhibits the covering fraction of Lyα absorbers that is lower than observed, we would be able to conclude that the excluded gas plays a major role in absorption. In addition, the complete analysis should be repeated for simulations with different feedback models to examine the sensitivity of the results to particular prescriptions. We will address these issues in our future publication.

We also studied the median H I Lyα optical depth of gas with given properties on relatively large scales in comparison with halo sizes ($\lesssim 5$ pMpc from the haloes), as a function of 3-D distance ($\equiv \sqrt{d_{\rm LOS}^2 + b^2}$, where $d_{\rm LOS}$ is the LOS separation between the halo and the absorber estimated from their velocity separation assuming that it is due to Hubble expansion). The main findings are:

- At large distances ($\gtrsim 1$ pMpc), gas with a maximum past temperature of $\lesssim 10^{5.5}$ K produces a median optical depth that is only $\lesssim 5\%$ lower than the total median optical depth (i.e. when we include all gas), suggesting that most of absorption in the Lyα forest is due to gas that was never shock-heated to high temperatures. This gas alone can account for the observed median optical depth at distances $\gtrsim 200$ pkpc.
- Gas within the haloes produces a median optical depth that is $\lesssim 20\%$ lower than that produced by all gas within ~ 130 pkpc (3-D distance), and its contribution to the total median optical depth is negligible beyond this distance.
- Gas that is inflowing towards the nearest halo with $M_{\rm h} > 10^{11.5} \mathrm{M}_{\odot}$ pro-

duces a median optical depth that is $\gtrsim 30\%$ lower than that produced by all particles within ~ 1 pMpc from the haloes; it remains significant even at 2 pMpc, beyond which static gas becomes dominant. This suggests that even at large distances, a non-negligible amount of gas is moving towards the haloes, which is a consequence of the ongoing structure formation. This is consistent with the observations of Rakic et al. (2011) who detected gas infall on scales of 1.4-2 pMpc from galaxies. The outflowing gas produces a median optical depth that is $\lesssim 1.5\%$ of that produced by all gas within ~ 1 pMpc and negligible beyond.

- Gas that will join the ISM of galaxies by $z = 0$ and is not in the ISM at $z = 2.25$, produces a median optical depth that is $\sim 30\%$ lower than that produced by all Lyα absorbing particles within ~ 130 pkpc. Its contribution to the median optical depth declines with distance from haloes, and is negligible beyond ~ 500 pkpc. The majority of this gas will accrete onto a galaxy for the first time. Most of the Lyα forest gas, however, does not come into galaxies before $z = 0$.

Finally, we looked at the overdensity and temperature of gas with a given optical depth, at different impact parameters from the haloes, using simulations where no radiative transfer post-processing was applied. We find:

- The *REF* model predicts that absorbers with optical depth $10^{-2} \lesssim \tau_{\mathrm{Ly}\alpha} \lesssim 10$ are typically produced by gas whose temperature and density follow the temperature-density relation, i.e. the temperature increases with the gas density. This relation changes closer to galaxies, and is almost fully inverted, i.e. gas temperature increases with decreasing density, within ~ 0.25 pMpc from haloes with $M_{\mathrm{h}} > 10^{11.5}\,\mathrm{M}_{\odot}$. This is mostly due to SN-driven winds heating the gas near galaxies. As a result, the physical properties of gas with the same Lyα optical depth change depending on where it is with respect to galaxies.
- The *AGN* model predicts a temperature-density relation that differs from the reference model even at ~ 2 pMpc from the haloes, with more gas heated to high temperatures. The relation is fully inverted (i.e. gas temperature increases with decreasing density) within ~ 1 pMpc.
- In the *NOSN* model the temperature-density relation appears largely independent of separation from haloes, but is slightly inverted within ~ 200 pkpc. This suggests that the galactic feedback is not solely responsible for the inversion, and that gravitational shock-heating plays a role as well.

The fact that the temperature-density relation appears sensitive to the feedback model, and that it changes as a function of distance from haloes, provides another way to constrain galactic feedback once observations of the temperature-density relation can be performed at different distances from galaxies. Although performed on larger scales, an indirect proof of concept is the measurement of the IGM temperature in the QSO proximity zone by Bolton et al. (2010). Their measurement was conducted across ≈ 30 cMpc in

a single sightline, while we found that strong feedback can impact the physical state of the IGM out to (at least) ~ 2 pMpc. While it will be difficult to test our predictions in a single sightline, a number of sightlines (QSO-galaxy pairs) passing at different distances from galaxies can make up sufficient redshift path for the temperature to be measured as a function of distance from galaxies (see Rudie et al., 2011, in preparation).

References

Adelberger K. L., Steidel C. C., Shapley A. E., Pettini M., 2003, ApJ, 584, 45
Adelberger K. L., Shapley A. E., Steidel C. C., Pettini M., Erb D. K., Reddy N. A., 2005, ApJ, 629, 636
Altay, G., Theuns, T., Schaye, J., Crighton, N. H. M., Dalla Vecchia, C., 2011, ApJ, 737, L37
Birnboim, Y., Dekel, A., 2003, MNRAS, 345, 349
Bolton, J. S., Becker, G. D., Wyithe, J. S. B., Haehnelt, M. G., & Sargent, W. L. W. 2010, MNRAS, 406, 612
Brooks, A. M., Governato, F., Quinn, T., Brook, C. B., Wadsley, J., 2009, ApJ, 694, 396
Bryan, G. L., & Norman, M. L. 1998, ApJ, 495, 80
Chen, Y.-M., Tremonti, C. A., Heckman, T. M., Kauffmann, G., Weiner, B. J., Brinchmann, J., Wang, J., 2010, AJ, 140, 445
Chabrier, G., 2003, PASP, 115, 763
Crain, R. A., Theuns, T., Dalla Vecchia, C., Eke, V. R., Frenk, C. S., Jenkins, A., Kay, S. T., Peacock, J. A., Pearce, F. R., Schaye, J., Springel, V., Thomas, P. A., White, S. D. M., Wiersma, R. P. C., 2009, MNRAS, 399.1773
Dalla Vecchia, C., Schaye, J., 2008, MNRAS, 387, 1431
Dijkstra M., Loeb, A., 2009, MNRAS, 400, 1109
Dolag, K., Borgani, S., Murante, G., Springel, V., 2009, MNRAS, 399, 497
Erb, D. K., Shapley, A. E., Pettini, M., et al. 2006, ApJ, 644, 813
Erb, D. K. 2008, ApJ, 674, 151
Faucher-Giguère, C.-A., Kereš, D., Dijkstra, M., Hernquist, L., Zaldarriaga, M., 2010, ApJ, 725, 633
Faucher-Giguere C.-A., Kereš D., 2011, MNRAS, 412, 118
Faucher-Giguere, C.-A., Kereš, D., Ma, C.-P., 2011, MNRAS, in press
Fumagalli, M., Prochaska, J. X., Kasen, D., Dekel, A., Ceverino, D., Primack, J. R., 2011, MNRAS, in press
Furlanetto, S. R., Schaye, J., Springel, V., & Hernquist, L. 2005, ApJ, 622, 7
Geach, J. E., Alexander, D. M., Lehmer, B. D., Smail, I., Matsuda, Y., Chapman, S. C., Scharf, C. A., Ivison, R. J., Volonteri, M., Yamada, T., Blain, A. W., Bower, R. G., Bauer, F. E., Basu-Zych, A., 2009, ApJ, 700, 1
Giavalisco, M., Vanzella, E., Salimbeni, S., Tripp, T. M., Dickinson, M., Cassata, P., Renzini, A., Guo, Y., Ferguson, H. C., Nonino, M., Cimatti, A., Kurk, J., Mignoli, M., Tang, Y., 2011, ApJ, in press
Goerdt, T., Dekel, A., Sternberg, A., et al., 2010, MNRAS, 407, 613
Haardt F., Madau P., 2001, in Neumann D. M., Tran J. T. V., eds, Clusters of Galaxies and the High Redshift Universe Observed in X-rays Modelling the UV/X-ray cosmic background with CUBA, arXiv: 0106018
Hayes, M., Scarlata, C., & Siana, B. 2011, Nature, 476, 304
Hui, L., & Gnedin, N. Y. 1997, MNRAS, 292, 27
Kereš, D., Katz, N., Weinberg, D. H., Davé, R., 2005, MNRAS, 363, 2
Kereš, D., Katz, N., Fardal, M., Davé, R., Weinberg, D. H., 2009, MNRAS, 395, 160
Kimm, T., Slyz, A., Devriendt, J., & Pichon, C. 2011, MNRAS, 413, L51
Lacey, C., & Cole, S. 1994, MNRAS, 271, 676
Martin, C. L., Bouché, N., 2009, ApJ, 703, 1394

Nilsson, K. K., Fynbo, J. P. U., Møller, P., Sommer-Larsen, J., Ledoux, C., 2006, A&A, 452, 23
Ocvirk, P., Pichon, C., Teyssier, R., 2008, MNRAS, 390, 1326
Oppenheimer, B. D., Davé, R., Kereš, D., et al. 2010, MNRAS, 406, 2325
Papovich, C., Finkelstein, S. L., Ferguson, H. C., Lotz, J. M., Giavalisco, M., MNRAS, 412, 1123
Pettini, M., Shapley, A. E., Steidel, C. C., Cuby, J.-G., Dickinson, M., Moorwood, A. F. M., Adelberger, K. L., Giavalisco, M., 2001, ApJ, 554, 981
Prochaska, J. X., Wolfe, A. M., 2009, ApJ, 696, 1543
Rakic, O., Schaye, J., Steidel, C. C., & Rudie, G. C. 2011, arXiv:1109.4944
Rauch M., et al., 1997, ApJ, 489, 7
Ribaudo, J., Lehner, N., Howk, J. C., Werk, J. K., Tripp, T. M., Prochaska, J. X. , Meiring, J. D., Tumlinson, J., 2011, ApJ, in press
Rubin K. H. R., Prochaska J. X., Koo D. C., Phillips A. C., Weiner B. J., 2010, ApJ, 712, 574
Schaye, J. 2001, ApJ, 559, 507
Schaye, J., Dalla Vecchia, C., Booth, C. M., Wiersma, R. P. C., Theuns, T., Haas, M. R., Bertone, S., Duffy, A. R., McCarthy, I. G., van de Voort, F., 2010, MNRAS, 402, 1536
Shapiro, K. L., Genzel, R., Quataert, E., Förster Schreiber, N. M., Davies, R., Tacconi, L., Armus, L., Bouché, N., Buschkamp, P., Cimatti, A., Cresci, G., Daddi, E.,Eisenhauer, F., Erb, D. K., Genel, S., Hicks, E. K. S., Lilly, S. J., Lutz, D., Renzini, A., Shapley, A., Steidel, C. C., Sternberg, A., ApJ, 701, 955
Steidel, C. C., Adelberger, K. L., Shapley, A. E., Pettini, M., Dickinson, M., Giavalisco, M., 2000, ApJ, 532, 170
Steidel C. C., Erb D. K., Shapley A. E., Pettini M., Reddy N., Bogosavljević M., Rudie G. C., Rakic O., 2010, ApJ, 717, 289
Steidel, C. C., Bogosavljević, M., Shapley, A. E., Kollmeier, J. A., Reddy, N. A., Erb, D. K., Pettini, M., 2011, ApJ, 736, 160
Stewart, K. R., Kaufmann, T., Bullock, J. S., Barton, E. J., Maller, A. H., Diemand, J., Wadsley, J., 2011,ApJ, 735, L1
Stewart, K. R., Kaufmann, T., Bullock, J. S., Barton, E. J., Maller, A. H., Diemand, J., Wadsley, J., 2011, ApJ, 738, 39
Van de Voort, F., Schaye, J., Booth, C. M., Haas, M. R., & Dalla Vecchia, C. 2011, MNRAS, 414, 2458
Van de Voort, F., Schaye, J., Booth, C. M., & Dalla Vecchia, C. 2011, MNRAS, 415, 2782
Van de Voort, F., Schaye, J., Altay, G., & Theuns, T. 2011, arXiv:1109.5700
Weiner et al., 2009, ApJ, 692, 187
Wiersma, R. P. C., Schaye, J., Smith, B. D., 2009. MNRAS, 393, 99
Wiersma, R. P. C., Schaye, J., Theuns, T., Dalla Vecchia, C., Tornatore, L., 2009, MNRAS, 399, 574